The current issue and full text archive of this journal is available at
www.emeraldinsight.com/0961-5539.htm

Received 1 September 2006
Revised 27 September 2007
Accepted 27 September 2007

A piecewise parabolic method for barotropic and nonbarotropic two-fluid flows

J.G. Zheng, T.S. Lee and S.H. Winoto
Department of Mechanical Engineering, National University of Singapore, Singapore, Singapore

Abstract

Purpose – The aim of the study is to present a piecewise parabolic method (PPM) for numerical simulation of barotropic and nonbarotropic two-fluid flows in more than one space dimension.

Design/methodology/approach – In transition layers of two components, a fluid mixture model system is introduced. Besides, conserving the mass, momentum and energy for the mixture, the model is supplemented with an advection equation for the volume fraction of one of the two fluid components to recover the pressure and track interfaces. The Tait and stiffened gas equations of state are used to describe thermodynamic properties of the barotropic and nonbarotropic components, respectively. To close the model system, a mixture equation of state is derived. The classical third-order PPM is extended to the two-fluid case and used to solve the model system.

Findings – The feasibility of this method has been demonstrated by good results of sample applications. Each of the material interfaces is resolved with two grid cells and there is no any pressure oscillation on the interfaces.

Research limitations/implications – With the mixture model system, there may be energy gain or loss for the nonbarotropic component on the material interfaces.

Practical implications – The method can be applied to a wide range of practical problems.

Originality/value – The method is simple. It not only has the advantage of Lagrangian-type schemes but also keeps the robustness of Eulerian schemes.

Keywords Simulation, Liquid flow, Mixtures, Compressible flow

Paper type Research paper

1. Introduction

Compressible multi-fluid flows with interfaces are involved in many applications from gas mixing for combustion to bubbly flow and Richtmyer-Meshkov instability (RMI). Usually, complex physics such as surface tension and heat conduction occur on the interfaces. Therefore, establishing numerical methods to simulate such flows is of importance.

Up to now, quite a few numerical approaches have been developed in both Lagrangian and Eulerian frameworks to deal with compressible multi-fluid flows. These approaches can be roughly categorized into four types: interface-tracking method, volume of fluid method, Level-set method, and spread interface method (Allaire *et al.*, 2002; Perigaud and Saurel, 2005). Here, the first three methods will not be described in detail and only the last one, i.e. the spread interface or mixture fluid method will be discussed. In the spread interface method, the interfaces are not accurately tracked, but are allowed to be smeared over a small number of cells, which means that there is a transition layer between two components separated by an interface.

International Journal of Numerical Methods for Heat & Fluid Flow
Vol. 18 No. 6, 2008
pp. 708-729

0961-5539
DOI 10.1108/09615530810885533

Accordingly, we face two challenges. First, we have to establish a model system that is able to correctly describe the behaviors of the mixture. Second, we need to find a way of obtaining consistent thermodynamic law for the mixture. Usually, researchers establish models based on the compressible Euler equations and supplement them with some extra equations to recover the thermodynamic states. In addition, mixture equations of state are defined to calculate the pressure for the mixtures and close the model systems. Abgrall (1996) proposed a basic principle for construction of oscillation-free schemes, i.e. fluids separated by an interface within a cell must have the same pressure. If this rule is not satisfied, pressure oscillations will occur on material interfaces. He applied this equilibrium pressure assumption to γ law gas flows. Later, Shyue (1998, 1999a, 2001), Ma *et al.* (2001) and Allaire *et al.* (2002) developed different methods based on this assumption.

However, the above methods are specially designed for nonbarotropic flows. For barotropic two-fluid flows, van Brummelen and Koren (2003) developed a pressure-invariant conservative Godunov-type method. Shyue (2004) proposed a volume-fraction based algorithm by viewing the mixture as a nonbarotropic fluid and deriving a nonisentropic equation of state (EOS). Shyue's scheme works well for a wide range of problems. He also developed a volume-fraction based method for hybrid barotropic and nonbarotropic two-fluid flow problems in which the mixture of two components was again assumed to be nonbarotropic (Shyue, 2006). However, a big challenge to Shyue's model is that the energy conservation for the nonbarotropic component cannot be maintained in the small neighborhood of the interface when a barotropic fluid is coupled to a nonbarotropic fluid. This issue is still open. Although theoretically there may be energy loss or gain on the interfaces, numerical tests show that the energy balance has almost no effect on the results. Here, energy balance implies energy conservation. Some of recent publications dealing with barotropic and nonbarotropic two-fluid flows are those of Johnsen and Colonius (2006), Nourgaliev *et al.* (2006), Liu *et al.* (2003, 2005) and Fedkiw *et al.* (1999).

This paper is concerned with the two-fluid flows where the material interface separates a barotropic fluid with Tait EOS and a nonbarotropic fluid with stiffened gas EOS. The two equations of state are widely used in various practical problems. For the pure barotropic fluid, the mass and momentum conservation equations together with Tait EOS are complete, while for the pure nonbarotropic fluid, the full set of Euler equations is used. To deal with the mixture, we employ a simplified five-equation model presented in Allaire *et al.* (2002). Besides, the basic conservation of the mass, momentum and energy, an advection equation for the volume fraction of one fluid component is supplemented to calculate the state variables and track material interfaces. Drawing on the idea in Shyue (2004, 2006), we derive a mixture EOS where the assumption of the equilibrium pressure is adopted. With this equation, the pressure of the mixture can be calculated and the model is complete.

Note that in the present model, physical effects such as surface tension, viscosity and heat transfer on the material interfaces are ignored. Another important phenomenon is that cavitation usually appears in the vicinity of the interface due to wave interaction with the interface. However, the present method does not allow for the cavitation because of the artificial modeling and treatment of the interface.

We employ the third-order piecewise parabolic method (PPM) to solve the proposed model system. This version of PPM is composed of the Lagrangian step and

remapping step. In the first step, the governing equations are evolved in the Lagrangian frame, while in the second step, the computed results in the previous step are mapped onto the fixed Eulerian grid, which combines the advantages of Lagrangian and Eulerian schemes into the present algorithm. At the same time, it is very easy to extend this scheme to multi-fluid cases and multidimensional implementations by using the dimensional-splitting technique. Numerical simulations have been done in one and multiple dimensions to verify this method. It is observed that our method is able to successfully deal with the barotropic and nonbarotropic two-fluid flows where clear material interfaces are captured and spurious oscillations in the pressure profile are eliminated.

This paper is organized as follows. In Section 2, the Tait and stiffened gas EOSs are described and a mixture EOS is derived. In Section 3, the mixture model system is introduced. In Section 4, PPM is discussed and then extended to the two-fluid flows and multiple dimensions. In Section 5, the calculations for some sample applications in one and two space dimensions are performed to validate our method. The conclusion is given in Section 6.

2. Equation of state

In this study, the thermodynamic properties of the barotropic fluids are described by the Tait EOS:

$$p(\rho) = (p_0 + \beta)\left(\frac{\rho}{\rho_0}\right)^{\gamma} - \beta \tag{1}$$

where p and ρ represent the pressure and density, respectively; p_0 denotes a reference pressure; β, a weak function of the entropy, is usually taken as a constant; γ is a dimensionless coefficient; and ρ_0 is the liquid density extrapolated to pressure p_0 (Thompson, 1972). Based on the first and second laws of thermodynamics, equation (1) can be rewritten as:

$$p(\rho) = (\gamma - 1)\rho e - \gamma\beta \tag{2}$$

where e is the internal energy per unit mass. However, the pressure in this expression is given by Tait EOS (1). The associated sound speed for fluids with Tait EOS is:

$$c = \sqrt{\left(\frac{\partial p}{\partial \rho}\right)_e + \frac{p}{\rho^2}\left(\frac{\partial p}{\partial e}\right)_\rho} = \sqrt{\frac{\gamma(p+\beta)}{\rho}}$$

But for the nonbarotropic fluids, we use the stiffened gas EOS:

$$p = (\gamma - 1)\rho e - \gamma p_\infty \tag{3}$$

Here, p, ρ and e are the pressure, density and internal energy, respectively; γ is the adiabatic coefficient and p_∞ is a material-dependent constant. Obviously, the stiffened gas EOS reduces to the perfect gas EOS as p_∞ is set to be zero, and thus it is suitable for both gases and liquids. The corresponding sound speed for the stiffened fluids is:

$$c = \sqrt{\frac{\gamma(p + p_\infty)}{\rho}}.$$

For a barotropic one-phase flow with the Tait EOS, the energy conservation equation can be decoupled from the mass and momentum conservation equations, as the pressure is the function of the density only. However, for a nonbarotropic one-phase flow, the complete set of Euler equations is applied. The spread interface method allows the material interface between two fluids to be smeared over a few grid cells. An artificial EOS should be developed in the transition layers between the two fluids. However, coupling a barotropic fluid to a nonbarotropic fluid is not trivial as the energy balance issue arises.

Shyue (2006) proposed a volume-fraction based algorithm for hybrid barotropic and nonbarotropic two-fluid flows. He viewed the mixture as a new nonbarotropic fluid and derived a mixture EOS. To construct the model, two assumptions are made. The first is that all the fluid components are in an adiabatic equilibrium with the same entropy. The second is that different components in a cell have the same pressure. Shyue's method suffers from a drawback, namely the energy conservation of the nonbarotropic fluid cannot be maintained in the vicinity of an interface. However, it seems that the problem of energy balance does not influence the numerical results presented in Shyue (2006).

In the present study, we also wish to build a mixture EOS by following Shyue's (2004, 2006) idea. Again, the mixture of the two fluids is assumed to be nonbarotropic, and then a generalized EOS is derived by combining equations (2) and (3):

$$p = (\gamma - 1)\rho e - \gamma(\beta + p_\infty) \tag{4}$$

It becomes equations (2) or (3) when p_∞ or β is set to be zero, respectively. However, in the transition layers, none of p_∞ and β is close to zero and thus equation (4) serves as an appropriate EOS for the mixture. In such case, p is not a function of the density ρ only, but is determined by two independent state variables, the density ρ and internal energy e. In addition, it is easy to show that the energy of each fluid component can be given by equation (4). But for the barotropic fluid, the pressure should be calculated from the Tait EOS (1). The mixture EOS (4) gives a way of recovering the pressure in the transition layers. The basic idea behind the equation is that the mixture is treated as a nonbarotropic fluid. A problem arising from this EOS is how to calculate the parameters γ, β and p_∞, which will be discussed in the next section.

3. Governing equations

A barotropic fluid flow is governed by the isentropic version of the compressible Euler equations:

$$\begin{cases} \frac{\partial \rho}{\partial t} + \frac{\partial(\rho u)}{\partial x} = 0 \\ \frac{\partial}{\partial t}(\rho u) + \frac{\partial}{\partial x}(\rho u^2 + p) = 0 \end{cases} \tag{5}$$

where ρ, p and u are the density, pressure and velocity, respectively. The energy conservation equation is ignored as the pressure depends only on the density, $p = p(\rho)$.

For a nonbarotropic fluid flow, the energy conservation equation should be supplemented:

$$\frac{\partial}{\partial t}(\rho E) + \frac{\partial}{\partial x}[(\rho E + p)u] = 0$$

Here, $E = (1/2)u^2 + e$ and e are the total and internal energy, respectively.

In the transition layers of the two fluids, a mixture model system is employed:

$$\begin{cases} \frac{\partial \rho}{\partial t} + \frac{\partial (\rho u)}{\partial x} = 0 \\ \frac{\partial}{\partial t}(\rho u) + \frac{\partial}{\partial x}(\rho u^2 + p) = 0 \\ \frac{\partial}{\partial t}(\rho E) + \frac{\partial}{\partial x}[(\rho E + p)u] = 0 \\ \frac{\partial Y^{(1)}}{\partial t} + u\frac{\partial Y^{(1)}}{\partial x} = 0 \end{cases} \tag{6}$$

where $Y^{(1)}$ is the volume fraction of fluid 1 with the constraints $Y^{(1)} \in [0, 1]$ and $Y^{(1)} + Y^{(2)} = 1$; ρ, u and $E = (1/2)u^2 + e$ are the density, velocity and total energy, defined as:

$$\rho = \sum_{i=1}^{2} Y^{(i)}\rho^{(i)}, \quad \rho u = \sum_{i=1}^{2} Y^{(i)}\rho^{(i)}u^{(i)} \tag{7a}$$

$$\rho E = \sum_{i=1}^{2}\left(Y^{(i)}\rho^{(i)}e^{(i)} + \frac{1}{2}\,Y^{(i)}\rho^{(i)}(u^{(i)})^2\right) \tag{7b}$$

Here, the quantities with the superscript (i) correspond to the relative states of fluid i. In the barotropic regions, $Y^{(1)} = 1$, while in the nonbarotropic regions $Y^{(1)}$ is set to be 0. In the transition layers, $Y^{(1)}$ takes the intermediate value between 0 and 1. Note that this model is also valid in the nonbarotropic fluid only regions, but the variables should be defined for the single fluid.

The model system (6) can be regarded as the 1D compressible Euler equations, except that it is supplemented with an advection equation for the volume fraction. In fact, it is the simplified five-equation model in Allaire *et al.* (2002), where the mass of each component is conserved. But in the current case, individual densities are not used in recovering the pressure; hence only the mass conservation equation for the mixture is included.

With EOS (4), model (6) is closed. Before calculating the parameters in equation (4), we introduce the assumption of equilibrium pressure, i.e. $p = p^{(1)} = p^{(2)}$. Here, it is assumed that the two fluid components within a cell have the same pressure. This assumption is critical as it can guarantee that our model is free of oscillations. In addition, there is no jump in velocity across a material interface, i.e. $u = u^{(1)} = u^{(2)}$. According to the EOS (4) and relation (7), the energy density for the mixture can be expressed as:

$$\frac{p + \gamma\beta + \gamma p_\infty}{\gamma - 1} = \rho e = \sum_{i=1}^{2} Y^{(i)}\rho^{(i)}e^{(i)} = \sum_{i=1}^{2} Y^{(i)}\left(\frac{p^{(i)} + \gamma^{(i)}\beta^{(i)} + \gamma^{(i)}p_\infty^{(i)}}{\gamma^{(i)} - 1}\right) \tag{8}$$

Here, the energy density of the mixture is the sum of those of individual fluids because each cell contains two components with different volume fractions. However, the introduction of the "fictitious energy" of the barotropic fluid will interfere with the energy balance of the nonbarotropic fluid. Therefore, as in Shyue (2006), the energy conservation of the nonbarotropic fluid is omitted in the small region near the material interface.

To solve for γ, β and p_∞, we split the above equality into the following three algebraic relations:

$$\frac{1}{\gamma-1}=\sum_{i=1}^{2}\frac{Y^{(i)}}{\gamma^{(i)}-1},\quad \frac{\gamma\beta}{\gamma-1}=\sum_{i=1}^{2}Y^{(i)}\frac{\gamma^{(i)}\beta^{(i)}}{\gamma^{(i)}-1},\quad \frac{\gamma p_\infty}{\gamma-1}=\sum_{i=1}^{2}Y^{(i)}\frac{\gamma^{(i)}p_\infty^{(i)}}{\gamma^{(i)}-1} \tag{9}$$

where the assumption of the equilibrium pressure $p=p^{(1)}=p^{(2)}$ has been used. Solving equation (9), we can obtain the values of γ, β and p_∞. So far, the model for the mixture is completely constructed and the next is to solve it efficiently. It should be remarked that though we adopt model (5) or (6) in different regions, the advection equation for the volume fraction is evolved in the whole domain. Its value can help us identify the component in each cell and further help us select the appropriate equations of motion as well as EOS in each portion of the computational domain.

The well-posedness of the model system (6) has not been carefully investigated in the literature. The problem is still open. Allaire *et al.* (2002) and Shyue (2006) only discussed some of elementary properties of the system.

4. Numerical method

PPM (Colella and Woodward, 1984a) is a third-order Godunov-type method. This method has several remarkable features that distinguish it from other Godunov-type schemes. First, the constant and linear interpolation functions used in Godunov's scheme and van Leer's MUSCL scheme, respectively, are replaced by a parabola, which allows for a more accurate representation of smooth spatial gradients, as well as a sharper profile of discontinuities, particularly contact discontinuities. Second, the representation of the nonlinear wave interactions used to calculate fluxes is greatly simplified, making the algorithm simpler and more robust. Third, additional dissipation is introduced to eliminate oscillations near shock waves and preserve stabilities. Finally, the Lagrangian-remapping version of PPM can be easily extended to multi-fluid flows and multidimensional implementation. These features make PPM highly suitable for multi-fluid problems with complex structures such as shock waves and contact discontinuities. Numerical tests prove that it outperforms other schemes (Colella and Woodward, 1984b). In this section, we first describe PPM by applying it to a linear advection equation, and then extend it to multi-fluid flows in multiple dimensions.

4.1 The PPM advection scheme

The construction of the parabolic interpolation function is very critical to PPM scheme. To describe this procedure clearly, we apply PPM to a linear advection equation:

$$\frac{\partial u}{\partial t}+a\frac{\partial u}{\partial x}=0;\quad u(x,0)=u_0(x),\quad a=\text{const} \tag{10}$$

Let $x_{j+1/2}$ be the boundary between the jth and $(j+1)$th cells, and assume that u_j^n is known. Here, u_j^n is the cell average of the accurate solution $u(x,t)$ in the jth cell $(x_{j-1/2},x_{j+1/2})$ at time $t=t_n$ and given by:

$$u_j^n=\frac{1}{\Delta x_j}\int_{x_{j-1/2}}^{x_{j+1/2}}u(x,t^n)\mathrm{d}x,\quad \Delta x=x_{j+1/2}-x_{j-1/2} \tag{11}$$

where Δx_j is the size of the jth cell, satisfying the stability condition $a\Delta t/\min_j \Delta x_j \leq 1$ with Δt representing the time step.

We construct the interpolation function $u(x)$, a piecewise continuous polynomial, in such a way that it satisfies the integration relation:

$$u_j^n = \frac{1}{\Delta x_j}\int_{x_{j-1/2}}^{x_{j+1/2}} u(x)\mathrm{d}x \tag{12}$$

Apparently, the solution of the advection equation (10) is $u(x, t^{n+1}) = u(x - a\Delta t, t^n)$, so we can explicitly calculate u_j^{n+1}, the cell average at a new time level $t^{n+1} = t^n + \Delta t$:

$$u_j^{n+1} = \frac{1}{\Delta x_j}\int_{x_{j-1/2}}^{x_{j+1/2}} u(x - a\Delta t)\mathrm{d}x \tag{13}$$

Therefore, what we need to do is to construct the interpolation function $u(x)$. PPM uses a parabolic function as the interpolation polynomial which takes the form:

$$\begin{aligned} u(x) &= u_{L,j} + \xi(\Delta u_j + u_{6,j}(1-\xi)) \\ \xi &= \tfrac{(x - x_{j-1/2})}{\Delta x_j}, \quad x_{j-1/2} \leq x \leq x_{j+1/2} \end{aligned} \tag{14}$$

where the coefficients are written as:

$$\begin{aligned} &\lim_{x \to x_{j-1/2}^+} u(x) = u_{L,j}, \qquad \lim_{x \to x_{j+1/2}^-} u(x) = u_{R,j} \\ &\Delta u_j = u_{R,j} - u_{L,j}, \quad u_{6,j} = 6\left(u_j^n - \tfrac{1}{2}(u_{L,j} + u_{R,j})\right) \end{aligned} \tag{15}$$

In smooth regions where the solution has no extrema, we have $u_{L,j+1} = u_{R,j} = u_{j+1/2}^n$. Here, $u_{j+1/2}^n$ is the approximation to $u(x)$ at the boundary $x_{j+1/2}$ and is interpolated by using a fourth degree polynomial:

$$\begin{aligned} u_{j+1/2}^n = u_j^n &+ \frac{\Delta x_j}{\Delta x_j + \Delta x_{j+1}}\left(u_{j+1}^n - u_j^n\right)\frac{1}{\sum_{k=-1}^{2}\Delta x_{j+k}} \\ &\times\left\{\frac{2\Delta x_j \Delta x_{j+1}}{\Delta x_j + \Delta x_{j+1}}\left[\frac{\Delta x_{j-1} + \Delta x_j}{2\Delta x_j + \Delta x_{j+1}} - \frac{\Delta x_{j+2} + \Delta x_{j+1}}{2\Delta x_{j+1} + \Delta x_j}\right]\left(u_{j+1}^n - u_j^n\right)\right. \\ &\left. - \Delta x_j \frac{\Delta x_{j-1} + \Delta x_j}{2\Delta x_j + \Delta x_{j+1}}\,\delta u_{j+1} + \Delta x_{j+1}\frac{\Delta x_{j+1} + \Delta x_{j+2}}{2\Delta x_{j+1} + \Delta x_j}\,\delta u_j\right\} \end{aligned} \tag{16}$$

where δu_j is the average slope in the jth cell of the parabola:

$$\delta u_j = \frac{\Delta x_j}{\Delta x_{j-1} + \Delta x_j + \Delta x_{j+1}}\left[\frac{2\Delta x_{j-1} + \Delta x_j}{\Delta x_j + \Delta x_{j+1}}\left(u_{j+1}^n - u_j^n\right) + \frac{2\Delta x_{j+1} + \Delta x_j}{\Delta x_{j-1} + \Delta x_j}\left(u_j^n - u_{j-1}^n\right)\right]$$

Colella and Woodward (1984a) modified δu_j, replacing it by $\delta_m u_j$:

$$\delta_m u_j = \begin{cases} \min\left(|\delta u_j|, 2\left|u_j^n - u_{j-1}^n\right|, 2\left|u_{j+1}^n - u_j^n\right|\right)\operatorname{sgn}(\delta u_j), \\ \text{if}(u_{j+1}^n - u_j^n)(u_j^n - u_{j-1}^n) > 0 \\ 0, \quad \text{otherwise} \end{cases}$$

This modification leads to a sharper profile of discontinuities in the solution, and also guarantees that $u_{j+1/2}^n$ lies in the range of values defined by u_j^n and u_{j+1}^n.

The value of $u_{j+1/2}^n$ calculated by the above procedure is third-order accurate for both uniform and nonuniform grids. $u_{j+1/2}^n$ will be assigned to $u_{L,j+1}$ and $u_{R,j}$ for most values of j. However, there are some cases where the interpolation function should be modified to improve the performance of this scheme. First, if values of the interpolation function fall out the range of values defined by $u_{L,j}$ and $u_{R,j}$, we should reset $u_{L,j}$ and $u_{R,j}$ to ensure the function is monotonic in each cell. Second, we modify the interpolation procedure slightly so that, in the neighborhood of a discontinuity, it produces a sharper profile than the scheme described above, i.e. if the jth cell is in a discontinuity, $u_{L,j}$ and $u_{R,j}$ should be reset. This is referred to as discontinuity detection and should be performed before applying the monotonicity algorithm. These modifications are complicated, so for simplicity we do not describe them here. For details, see the paper of Colella and Woodward (1984a).

Once the values of $u_{L,j}$ and $u_{R,j}$ are known, it is easy to evaluate u_j^{n+1} by integrating equation (14). We define averages of the interpolation function:

$$f_{j+1/2,L}^u(y) = \frac{1}{y}\int_{x_{j+1/2}-y}^{x_{j+1/2}} u(x)\mathrm{d}x, f_{j+1/2,R}^u(y) = \frac{1}{y}\int_{x_{j+1/2}}^{x_{j+1/2}+y} u(x)\mathrm{d}x \tag{17}$$

where y is assumed to be positive.

Substituting $u(x)$ given in equation (14) into the above formula yields:

$$\begin{aligned} f_{j+1/2,L}^u(y) &= u_{R,j} - \tfrac{\eta}{2}\left(\Delta u_j - \left(1 - \tfrac{2}{3}\eta\right)u_{6,j}\right), \qquad \eta = \tfrac{y}{\Delta x_j} \\ f_{j+1/2,R}^u(y) &= u_{L,j+1} + \tfrac{\eta}{2}\left(\Delta u_{j+1} + \left(1 - \tfrac{2}{3}\eta\right)u_{6,j+1}\right), \quad \eta = \tfrac{y}{\Delta x_{j+1}} \end{aligned} \tag{18}$$

Then, u_j^{n+1} can be expressed in explicit conservation form as:

$$u_j^{n+1} = u_j^n - \frac{\Delta t}{\Delta x_j}(\hat{f}_{j+1/2} - \hat{f}_{j-1/2}) \tag{19}$$

where the fluxes $\hat{f}_{j-1/2}$ and $\hat{f}_{j+1/2}$ are given by:

$$\hat{f}_{j+1/2} = \begin{cases} a f_{j+1/2,L}^u(a\Delta t), & \text{if } a \geq 0 \\ a f_{j+1/2,R}^u(-a\Delta t), & \text{if } a \leq 0 \end{cases} \tag{20}$$

From the above procedure for the linear advection equation, we can understand that one key element of PPM is to construct a parabolic interpolation function and adjust relative parameters to maintain monotonicity and treat discontinuities.

4.2 The PPM for compressible barotropic and nonbarotropic two-fluid flows

PPM is originally designed for the single fluid flows. In Colella and Woodward (1984a), two versions of this scheme are provided, i.e. Eulerian and Lagrangian-remapping formulations. In our paper, the latter is employed as it is third-order accurate and can be quite easily extended to the multi-fluid flows. Thus, calculations are first performed in the Lagrangian coordinate system and then the obtained results are mapped onto the fixed Eulerian grid. This version of PPM is highly suitable for problems where we are concerned with the material interfaces capturing. Though systems of equations (5) and (6) are solved in different regions, we only discuss equation (6) in this subsection because solving equation (5) is easier by following the same procedure.

In the Lagrangian coordinate system, the governing equations (6) are rewritten as:

$$\begin{cases} \frac{\partial \tau}{\partial t} - \frac{\partial (r^{\alpha} u)}{\partial m} = 0 \\ \frac{\partial u}{\partial t} + r^{\alpha} \frac{\partial p}{\partial m} = 0 \\ \frac{\partial E}{\partial t} + \frac{\partial (r^{\alpha} u p)}{\partial m} = 0 \\ \frac{\partial Y^{(i)}}{\partial t} = 0 \end{cases} \tag{21}$$

Here, u, p and E are the velocity, pressure, and total energy per unit mass, respectively; $Y^{(1)}$ is the volume fraction of fluid 1 and $\tau = 1/\rho$ is the specific volume; m is the mass coordinate satisfying the relation:

$$m(r) = \int_{r_0}^{r} \rho(r) r^{\alpha} \mathrm{d}r$$

where r is the spatial coordinate; $\alpha = 0, 1, 2$ correspond to the planar, cylindrical and spherical symmetry, respectively. At time t^n, we define the mass-weighted average of the quantity U as:

$$U_j^n = \frac{1}{\Delta m_j} \int_{m_{j-1/2}}^{m_{j+1/2}} U(m, t^n) \mathrm{d}m$$

with $U = (\rho, u, E, Y^{(1)})$.

The procedure of solving the model (21) consists of the following six steps:

(1) From the known cell averages ρ_j^n, u_j^n, E_j^n and $(Y^{(1)})_j^n$, we can calculate the pressure p_j^n using the EOS (4), i.e. $p_j^n = p(\rho_j^n, e_j^n, (Y^{(1)})_j^n)$ with $e_j^n = E_j^n - (1/2)(u_j^n)^2$.

(2) Apply the interpolation procedure described in the previous subsection to the cell averages ρ_j^n, u_j^n, p_j^n and $(Y^{(1)})_j^n$ to construct the corresponding interpolation functions $\rho(x)$, $u(x)$, $p(x)$ and $Y^{(1)}(x)$.

(3) With formula (18), we can construct the left and right states for a Riemann problem at the boundary $m = m_{j+1/2}$, i.e. $(\hat{\rho}_{j+1/2}, \hat{u}_{j+1/2}, \hat{p}_{j+1/2}, (\hat{Y}^{(1)})_{j+1/2})$ with $l = L, R$. Here, the left state is the average values of the dependent variables over the domain between $m_{j+1/2}$ and the point where the C^+ characteristic line $\mathrm{d}m/\mathrm{d}t = r^{\alpha}\rho c$ through $(m_{j+1/2}, t^{n+1})$ intersects the line $t = t^n$. The characteristic velocity is:

$$a_j = (r^{\alpha}\rho c)_j = \frac{\left(r^n_{j+1/2}\right)^{\alpha+1} - \left(r^n_{j-1/2}\right)^{\alpha+1}}{(\alpha+1)(r^n_{j+1/2} - r^n_{j-1/2})}\rho^n_j c^n_j$$

Thus, for the velocity we have:

$$\hat{u}_{j+1/2,L} = u_{R,j} - \frac{\eta}{2}\left(\Delta u_j - \left(1 - \frac{2}{3}\eta\right)u_{6,j}\right) \quad \eta = \frac{a_j \Delta t}{\Delta m_j}, \quad \Delta u_j = u_{R,j} - u_{L,j} \tag{22}$$

and other variables can be obtained in a similar manner. Similarly, the right state is the average values over the region between $m_{j+1/2}$ and the point where the C^- characteristic line $\mathrm{d}m/\mathrm{d}t = -r^{\alpha}\rho c$ through $(m_{j+1/2}, t^{n+1})$ intersects the line $t = t^n$. The characteristic velocity is taken as $-a_{j+1}$, so for the velocity we have:

$$\begin{aligned} &\hat{u}_{j+1/2,R} = u_{L,j+1} + \frac{\eta}{2}\left(\Delta u_{j+1} + \left(1 - \frac{2}{3}\eta\right)u_{6,j+1}\right) \quad \eta = \frac{a_{j+1}\Delta t}{\Delta m_{j+1}}, \\ &\Delta u_{j+1} = u_{R,j+1} - u_{L,j+1} \end{aligned} \tag{23}$$

The remaining variables can be calculated by taking the same procedure. In these expressions:

$$c = \sqrt{\frac{\gamma(p + \beta + p_{\infty})}{\rho}}$$

is the sound speed of the mixture.

(4) Solving a Riemann problem with the initial states calculated in the previous step, we can obtain the time-averaged values for $u^*_{j+1/2}$ and $p^*_{j+1/2}$ at the boundary $m = m_{j+1/2}$. The approximate Riemann solver will be discussed in detail in the next subsection.

(5) Evolve the governing equations (21) in the Lagrangian frame:

$$\begin{cases} x^{n+1}_{j+1/2} = x^n_{j+1/2} + \Delta t u^*_{j+1/2} \\ \tau^{n+1}_j = \dfrac{\left(x^{n+1}_{j+1/2}\right)^{\alpha+1} - \left(x^{n+1}_{j-1/2}\right)^{\alpha+1}}{(\alpha+1)\Delta m_j} \\ u^{n+1}_j = u^n_j + \frac{1}{2}(\bar{A}_{j+1/2} + \bar{A}_{j-1/2})\frac{\Delta t}{\Delta m_j}\left(p^*_{j-1/2} - p^*_{j+1/2}\right) \\ E^{n+1}_j = E^n_j + \frac{\Delta t}{\Delta m_j}\left(\bar{A}_{j-1/2}u^*_{j-1/2}p^*_{j-1/2} - \bar{A}_{j+1/2}u^*_{j+1/2}p^*_{j+1/2}\right) \\ (Y^{(1)})^{n+1}_j = (Y^{(1)})^n_j \end{cases} \tag{24}$$

where:

$$\bar{A}_{j+1/2} = \frac{\left[\left(x_{j+1/2}^{n+1}\right)^{\alpha+1} - \left(x_{j+1/2}^{n}\right)^{\alpha+1}\right]}{\left[(\alpha+1)\left(x_{j+1/2}^{n+1} - x_{j+1/2}^{n}\right)\right]}$$

(6) Finally, map the results obtained in the Lagrangian step onto the fixed Eulerian grid. Let $x_{j+1/2}^{0}$ be the Eulerian coordinate of the boundary $x_{j+1/2}$ at time t^n and $x_{j+1/2}^{n+1}$ be its Lagrangian coordinate at time t^{n+1}. The displacement of the boundary is $x_{j+1/2}^{*} = x_{j+1/2}^{n+1} - x_{j+1/2}^{0}$. Besides, V_j^0 is the volume of the fixed jth cell in the Eulerian frame at t^n, while V_j is the volume of the jth cell in the Lagrangian reference frame at t^{n+1}. $\Delta V_{j+1/2}^{*}$ denotes the volume of the mixture that passes through the boundary $x_{j+1/2}^{0}$. We apply the PPM interpolation and integration procedures to calculate:

$$U_{j+1/2}^{*} = \left(\rho_{j+1/2}^{*}, u_{j+1/2}^{*}, p_{j+1/2}^{*}, (Y^{(1)})_{j+1/2}^{*}\right)$$

$$U_{j+1/2}^{*} = \begin{cases} f_{j+1/2,L}^{U}\left(\frac{\Delta x_{j+1/2}^{*}}{\Delta x_j}\right) & \text{if } \Delta x_{j+1/2}^{*} \geq 0 \\ f_{j+1/2,R}^{U}\left(\frac{-\Delta x_{j+1/2}^{*}}{\Delta x_{j+1}}\right) & \text{if } \Delta x_{j+1/2}^{*} \leq 0 \end{cases} \tag{25}$$

Then the values of γ^*, β^* and p_∞^* can also be calculated. Define some quantities:

$$\Delta m_j = \rho_j V_j, \quad \Delta m_j^0 = (\rho_{\text{Euler}})_j V_j^0, \quad \Delta m_{j+1/2}^{*} = \rho_{j+1/2}^{*} \Delta V_{j+1/2}^{*}$$

$$\Delta E_{j+1/2}^{*} = \tfrac{1}{2}\left(u_{j+1/2}^{*}\right)^2 \Delta m_{j+1/2}^{*} + \left(\frac{p^* + \gamma^* \beta^* + \gamma^* p_\infty^*}{\gamma^* - 1}\right) \Delta V_{j+1/2}^{*}$$

Here, ρ_j and $(\rho_{\text{euler}})_j$ represent the densities in the Eulerian frame at times t^n and t^{n+1}, respectively. With those above, the remapping formulae are written as:

$$\begin{cases} (\rho_{\text{euler}})_j = \frac{\left[\Delta m_j + \rho_{j-1/2}^{*} \Delta V_{j-1/2}^{*} - \rho_{j+1/2}^{*} \Delta V_{j+1/2}^{*}\right]}{V_j^0} \\ (u_{\text{euler}})_j = \frac{\left[u_j \Delta m_j + u_{j-1/2}^{*} \Delta m_{j-1/2}^{*} - u_{j+1/2}^{*} \Delta m_{j+1/2}^{*}\right]}{\Delta m_j^0} \\ (E_{\text{euler}})_j = \frac{\left[E_j \Delta m_j + \Delta E_{j-1/2}^{*} - \Delta E_{j+1/2}^{*}\right]}{\Delta m_j^0} \\ [(Y^{(1)})_{\text{euler}}]_j = \frac{\left[(Y^{(1)})_j V_j + (Y^{(1)})_{j-1/2}^{*} \Delta V_{j-1/2}^{*} - (Y^{(1)})_{j+1/2}^{*} \Delta V_{j+1/2}^{*}\right]}{V_j^0} \end{cases} \tag{26}$$

where the variables on the left hand side denote the required solutions in the Eulerian coordinate system at the new time level t^{n+1}.

4.3 Riemann solver

In the PPM scheme, a key element is to efficiently solve Riemann problems because we must use their solutions to evolve the governing equations. To save computational efforts and improve efficiency, quite a few approximate Riemann solvers have been developed (Colella and Glaz, 1985; Toro, 1999). Here, we employ a two-shock approximation of the Riemann solver where rarefaction waves are neglected and replaced by shocks (Toro, 1999; Shyue, 1999a). In one space dimension, the constructed solution is composed of a rightward-going shock wave, a leftward-going shock wave and a contact discontinuity between them. Our aim is to find the midstate (u^*, p^*), the velocity and pressure in the region bounded by the left and right shock waves.

It is well known that solving the following nonlinear equations yields (u^*, p^*):

$$u_L^*(p^*) - u_R^*(p^*) = 0 \tag{27a}$$

$$u_L^*(p^*) = u_L - \frac{p^* - p_L}{M_L(p^*)}, \quad u_R^*(p^*) = u_R + \frac{p^* - p_R}{M_R(p^*)} \tag{27b}$$

where $u_L^*(p^*)$ and $u_R^*(p^*)$ satisfy the shock jump relations. On the other hand, based on the Rankine-Hugoniot jump condition:

$$M_l^2(e_l^* - e_l) = \frac{(p^*)^2 - p_l^2}{2}, \quad l = L \text{ or } R \tag{28}$$

the density jump relation across the shock waves:

$$\rho_l^*(p^*) = \begin{cases} \left[\rho_l^{-1} - \frac{p^* - p_l}{M_l^2(p^*)}\right]^{-1}, & Y^{(1)} \in [0,1) \\ \rho_{0l}\left(\frac{p^* + \beta_l}{p_{0l} + \beta_l}\right)^{1/\gamma_l}, & Y^{(1)} = 1 \end{cases} \tag{29}$$

as well as the EOS, an explicit expression for M_l can be derived:

$$M_l^2(p^*) = \begin{cases} C_l^2\left[1 + \frac{\gamma_l + 1}{2\gamma_l}\left(\frac{p^* + \beta_l + (p_\infty)_l}{p_l + \beta_l + (p_\infty)_l} - 1\right)\right], & Y^{(1)} \in [0,1) \\ -\frac{p^* - p_l}{(\rho_l^*)^{-1} - \rho_l^{-1}}, & Y^{(1)} = 1 \end{cases} \tag{30}$$

where $C_l = \rho_l c_l$ is the Lagrangian sound speed and c_l is the real sound speed.

Applying the secant method to equation (27a), we have the following iteration scheme:

$$(p^*)^{n+1} = (p^*)^n - \frac{\left|(p^*)^n - (p^*)^{n-1}\right|}{\left|(u_L^*)^n - (u_L^*)^{n-1}\right| + \left|(u_R^*)^n - (u_R^*)^{n-1}\right|}\left[(u_R^*)^n - (u_L^*)^n\right] \tag{31}$$

where n denotes iteration times. With the appropriate initial values of $(p^*)^0, (p^*)^1$, equations (27b) and (31) fast converge to the desired solution.

4.4 Multidimensional implementations

It is very easy to extent the one-dimensional PPM to multidimensional implementations by applying the operator splitting technique of Strang (1968). For example, in three space dimensions, calculations are performed as follows:

$$U^{n+1} = L_x(\Delta t)L_y(\Delta t)L_z(\Delta t)U^n$$
$$U^{n+2} = L_z(\Delta t)L_y(\Delta t)L_x(\Delta t)U^{n+1} \tag{32}$$

Here, L_x, L_y, L_z denote the PPM operators in the x, y and z directions, respectively. U is a vector with six unknowns as its elements. In fact, a 3D problem is decomposed into three 1D ones.

5. Numerical results

In order to validate the PPM scheme, we apply it to several problems in one and two dimensions, comparing numerical results with those in some references and examining its performance. Throughout calculations below, the courant number is set to be 0.6, i.e. Court $= 0.6$.

5.1 One-dimensional problems

Example 1. In this example, we present the simulation of a two-fluid Riemann problem. In the region $x \in [-2, 0)$, we have the nonbarotropic air characterized by the stiffened gas EOS with the initial state $(p, \rho, u; \gamma, p_\infty) = (1,000, 0.13895, 0; 1.4, 0)$, while in the region $x \in [0, 2]$, we have the barotropic water characterized by the Tait EOS with the initial state $(p, \rho, u; \gamma, \rho_0, p_0, \beta) = (1, 1, 0; 7, 1, 1, 3,000)$. In this calculation, a 200-cell grid is used and the results at time $t = 0.01$ are shown in Figure 1.

This example was first studied in Shyue (2004) where both water and air were assumed to be barotropic. Obviously, the self-similar solution consists of a rightward-going shock wave, a leftward-going rarefaction wave and a contact discontinuity between them. We can clearly see such structures in Figure 1 where both the computational and exact solutions are shown. On the material interface, the numerical diffusion is very small and no pressure oscillations occur. The numerical results compare quite well to the exact solution, which proves the validity of our method for the Riemann problem with a strong shock.

It should be noted that, in this paper, the exact solution of the 1D problem is not that to the model system (6). In the barotropic region, it is the exact solution to the isentropic version of the Euler equations, while in the nonbarotropic region, it corresponds to the solution to the full set of Euler equations.

To verify the convergence, we present the numerical results with four sets of grids: 200, 1,000, 5,000 and 10,000. As show in Figure 2, the results converge as the grids are refined.

Example 2. Now, we consider a more complicated case where a material interface will be accelerated by a shock. The computational domain is still $x \in [-2, 2]$, but unlike the above problem, the initial condition of this case is composed of three states. A material interface is located at the center of the domain. Water is on the left of the interface, while the right portion is occupied by air. In addition, in water, a traveling shock is located at $x = 0$ and moving from left to right, which means that the shock would collide with the material interface at time $t = 0$. We still use the Tait EOS for water and the stiffened gas EOS for air. The initial condition reads:

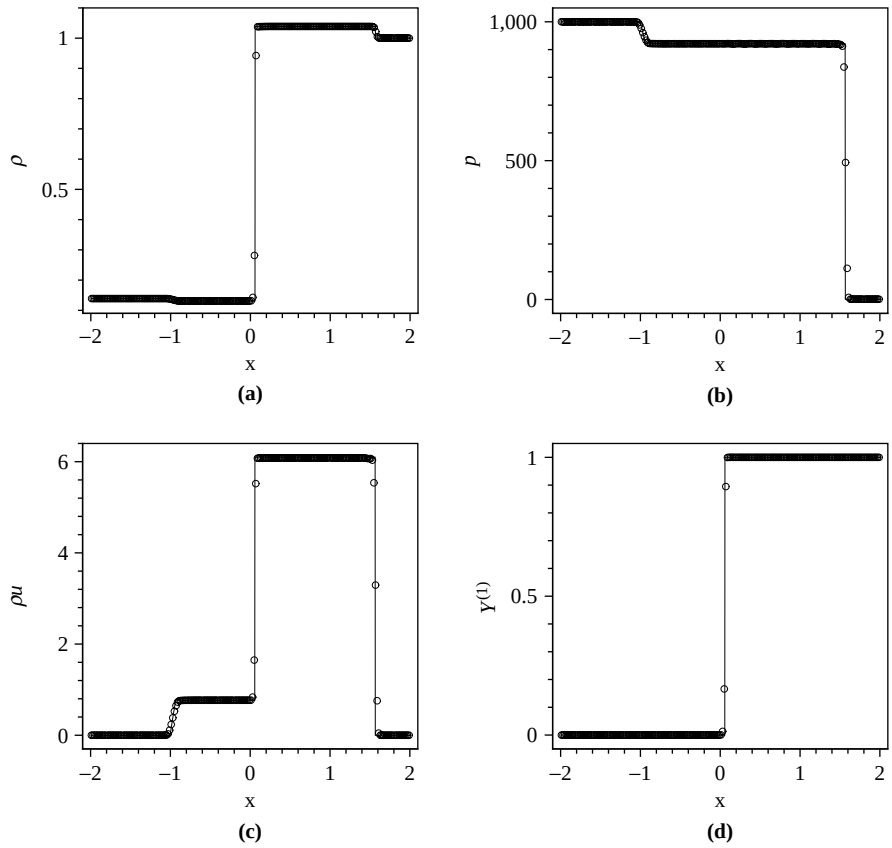

Notes: The four subfigures are (a) density; (b) pressure; (c) momentum and (d) volume fraction of water. The solid lines represent the exact solution, while the circles give the results by PPM with a uniform 200-cell grid

Figure 1.
Results of a two-fluid Riemann problem at time $t = 0.01$

$$(p, \rho, u; \gamma, \rho_0, p_0, \beta)_L = (10,\ 1.00043,\ 0.062;\ 7,\ 1,\ 1,\ 3,000)$$

$$(p, \rho, u; \gamma, \rho_0, p_0, \beta)_M = (1,\ 1,\ 0;\ 7,\ 1,\ 1,\ 3,000), (p, \rho, u; \gamma, p_\infty)_R = (1,\ 0.001,\ 0;\ 1.4,\ 0)$$

where quantities with subscripts L and R represent states of the fluids in the left and right sides of the domain, respectively; variables with subscript M give condition of the undisturbed water and are related to the left state by the shock and the right state by the contact discontinuity.

The results of this simulation at time $t = 0.01$ are shown in Figure 3. To show them more clearly, the logarithm scale is used in the density and pressure profiles. The PPM gives sharper representations of the shock wave and contact discontinuity, and the reflected rarefaction wave is also well calculated. As compared with other methods, our approach has the higher-order accuracy in smooth regions of the solution, and less diffusion near discontinuities. The material interface is captured accurately and there

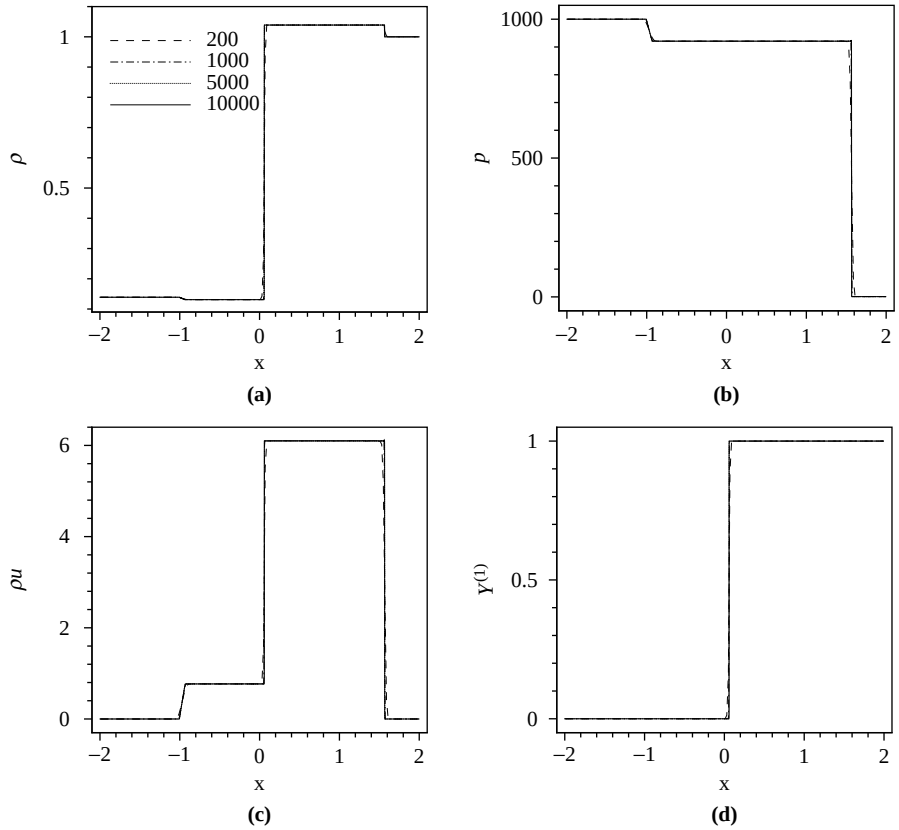

Figure 2.
Results of the Riemann problem shown in Figure, 1

Notes: The four subfigures are (a) density; (b) pressure; (c) momentum and (d) volume fraction of water. To study the convergence, we use four sets of grid: 200, 1000, 5000 and 10000

is no any pressure oscillation in vicinity of the interface. Again, the computational results agree quite well with the exact solution.

5.2 Two-dimensional problems

Example 3. This example is about the advection of a material interface separating two fluids. Initially, the center of a bubble of radius $r_0 = 0.16$ is located at $(x, y) = (0.25, 0.25)$ in the physical domain $[0, 1] \times [0, 1]$. Inside the bubble, we have the water with the state $(p, \rho; \gamma, \rho_0, p_0, \beta) = (1, 1; 7, 1, 1, 3, 000)$, while in the region outside the bubble, we have a gas with the state $(p, \rho; \gamma, p_\infty) = (1, 0.001; 1.4, 0)$. Unlike the problem in Shyue (2004) where both the two fluids are characterized by the Tait EOS, we use the Tait EOS for the water and the stiffened gas EOS for the gas in the current case. Since the two fluids are traveling with an equilibrium pressure $p = 1$ and a constant velocity $(u, v) = (100, 100)$, only a material interface exists. In this calculation, a 100×100 grid is used.

This example is taken from Shyue's (2004) paper and used here to confirm that our scheme can preserve the pressure invariance. Theoretically, this problem is very

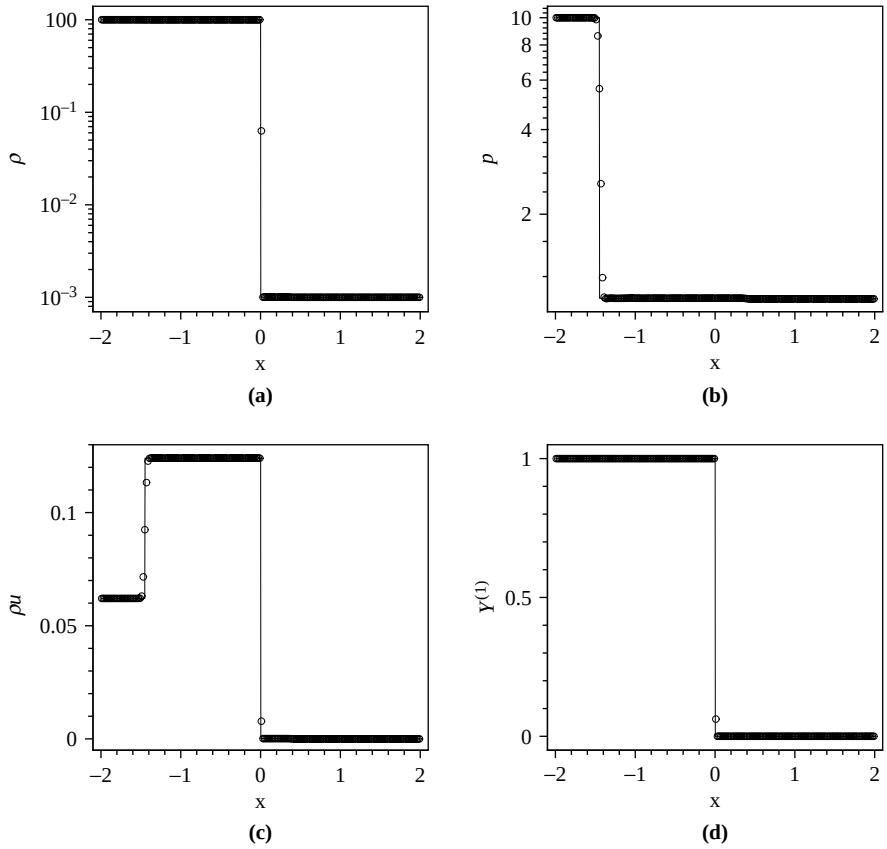

Notes: The four subfigures are (a) density (logarithm scale); (b) pressure (logarithm scale); (c) momentum and (d) volume fraction of water. The solid and circular lines denote the exact and computational solutions at time $t = 0.01$ respectively

Figure 3.
Results of a shock interaction with a material interface

simple and the interface should translate with the constant pressure and velocity. We run the code to the time of $t = 0.005$, and the corresponding results are shown in Figures 4 and 5. As shown in Figure 4, the air bubble remains circular and clear at the late time. Figure 5 shows the profiles of the density, pressure, velocity and volume fraction of water along the diagonal $y = x$. From this figure we can see that the computational results agree well with the exact solution, and the interface is well located. In addition, there is no any oscillation in pressure near the interface. As compared with that in Shyue (2004) where the transition layer is in over eight cells, the numerical diffusion is greatly reduced and the interface is captured within two cells. Although the comparison between the two different systems may be not appropriate, it serves as an example showing that our method can capture the material interface with small diffusion. This sample application demonstrates that our scheme works well for a pure interface problem with two different barotropic and nonbarotropic fluids.

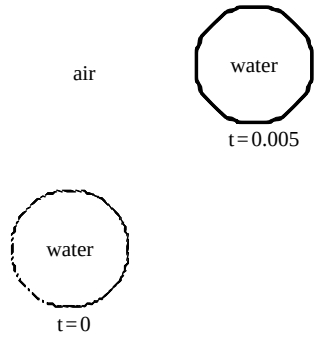

Note: In this calculation, a 100 × 100 grid is used

Figure 4.
Density contours of 2D material interface advection problem at time $t = 0, 0.005$

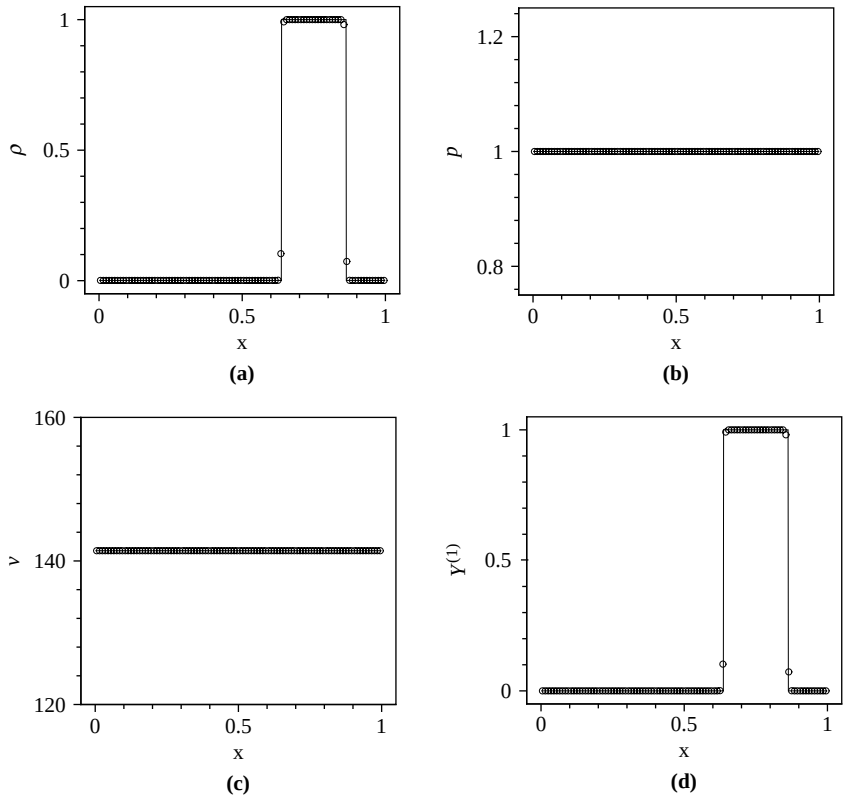

Notes: (a) Density; (b) pressure; (c) velocity; (d) volume fraction of water. Here the velocity v is defined as $v=\sqrt{u^2 + v^2}$. The solid lines denote the exact solution, while circles give the numerical results obtained by the PPM with a uniform 100 × 100 grid

Figure 5.
Results of the relevant variables along the diagonal $y = x$ at time $t = 0.005$ for the problem shown in Figure 4

Example 4. Now, we present a numerical simulation of RMI in two space dimensions. It is well known that in such problems, a material interface with small perturbation will become unstable when an incident shock in one fluid drives it, i.e. the amplitude of the perturbation varies with time. The two fluids separated by the interface have different densities and may be characterized by two distinct equations of state. In this example, the computational domain is selected as a rectangle with the size $[0,4]\times[0,1]$. The stationary interface is written as $x = x_0 + \varepsilon\cos(2\pi y)$, $y \in [0,1]$. Here, $x_0 = 1.2$ is the position of the unperturbed interface and $\varepsilon = 0.1$ is the amplitude of the perturbation. On the left of the interface, the fluid is a liquid with the state $(p, \rho, u; \gamma, p_\infty) = (1, 5, 0; 4, 0)$, while on the right of the interface, the fluid is a gas with the state $(p, \rho, u; \gamma, \rho_0, p_0, \beta) = (1, 1, 0; 1.4, 1, 1, 0)$. In the liquid, a rightward-going Mach 1.95 shock is located at $x = -1.5$. Besides, we suppose that the liquid is nonbarotropic and use the stiffened gas EOS for it, while for the gas, we use the Tait EOS.

After the interaction between the shock and interface, there will be a transmitted shock and a reflected rarefaction wave since the shock is originally located in the heavy fluid. We can observe the process of the interface evolution in Figure 6: at time $t = 0$, it is stationary with a specified perturbation, at time $t = 0.2$ the shock just penetrates the interface, at time $t = 1.2$ the phase inverse of the perturbation has completed and amplitude continues increasing, and at time $t = 2.0$, typical spike and bubble structures characteristic of RMI completely forms. Variations of amplitude and growth rate of the perturbation with time are shown in Figure 7. Here, the perturbation amplitude and growth rate are defined as $a = x_{\max} - x_{\min}$ and $v = \dot{x}_{\max} - \dot{x}_{\min}$, respectively, where x denotes the x coordinate of any point on the interface. We can observe the amplitude first decreases and then increases due to the effect of the phase inverse. Accordingly, the growth rate is negative, then becomes positive, and finally tends to a constant. Figure 8 shows the cross-sectional results of the density and pressure along the horizontal center line $y = 0.5$. To examine the convergence of numerical solutions, we do the simulation using three different sets of mesh grids, i.e. 100×25, 200×50 and 400×100. It is obvious that the solutions converge as the grids are refined. This calculation proves that our scheme can successfully capture the

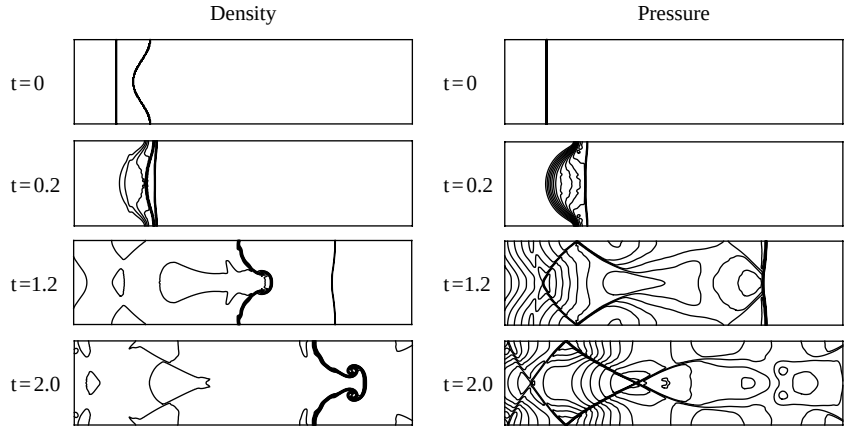

Note: The numerical results are obtained by PPM scheme with a 400 × 100 mesh grid

Figure 6.
Density and pressure contours of Richtmyer-Meshkov instability where a liquid-gas interface is driven by a Mach 1.95 shock in the liquid

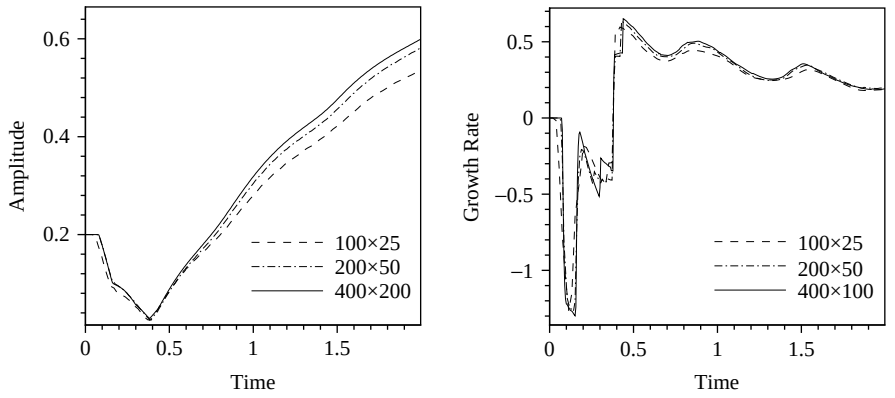

Figure 7.
The perturbation amplitude and growth rate

Note: Three sets of mesh grids are used to study convergence of the numerical solutions

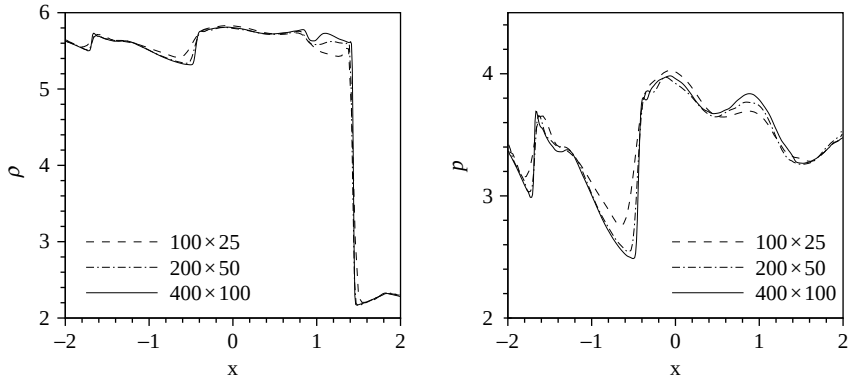

Figure 8.
Cross-sectional plots of the density and pressure along the horizontal center line $y = 0.5$ at time $t = 2.0$

Note: The number of grids used are 100×25, 200×50 and 400×100

2D interface between two thermodynamically different fluids in presence of shocks. In addition, to learn more about the RMI, see the review of Brouillette (2002).

Example 5. The final example concerns a shock wave in water interaction with an air bubble. In a rectangular domain $[0, 1] \times [-0.2, 1]$, a stationary air bubble of radius $r = 0.2$ is located at $(x_0, y_0) = (0.5, 0.5)$. The initial condition for air with stiffened gas EOS is $(p, \rho; \gamma, p_\infty) = (1, 0.0012; 1.4, 0)$. The bubble is surrounded by stationary water with the state $(p, \rho; \gamma, \rho_0, p_0, \beta) = (1, 1; 7, 1, 1, 3,000)$. Here, water is taken to fulfill Tait EOS. We assume that there is a downward-going Ma 1.587 shock in water on plane $y = 0.8$ located just over the bubble, and the corresponding post-shock state reads $(p, \rho, u, v; \gamma, \rho_0, p_0, \beta) = (10,000, 1.233, 0, -43.467; 7, 1, 1, 3,000)$. In this case, ratio of Lagrangian sound speed $(\rho c)_{\text{water}}/(\rho c)_{\text{air}} \approx 3,535$ is so large that simulation is more difficult.

This calculation is performed with a 200×240 mesh grid. Figure 9 shows contours of the density, pressure and volume fraction at three times $t = 0.001, 0.003$ and 0.005, demonstrating evolution of the bubble. At time $t = 0.001$, the shock wave is

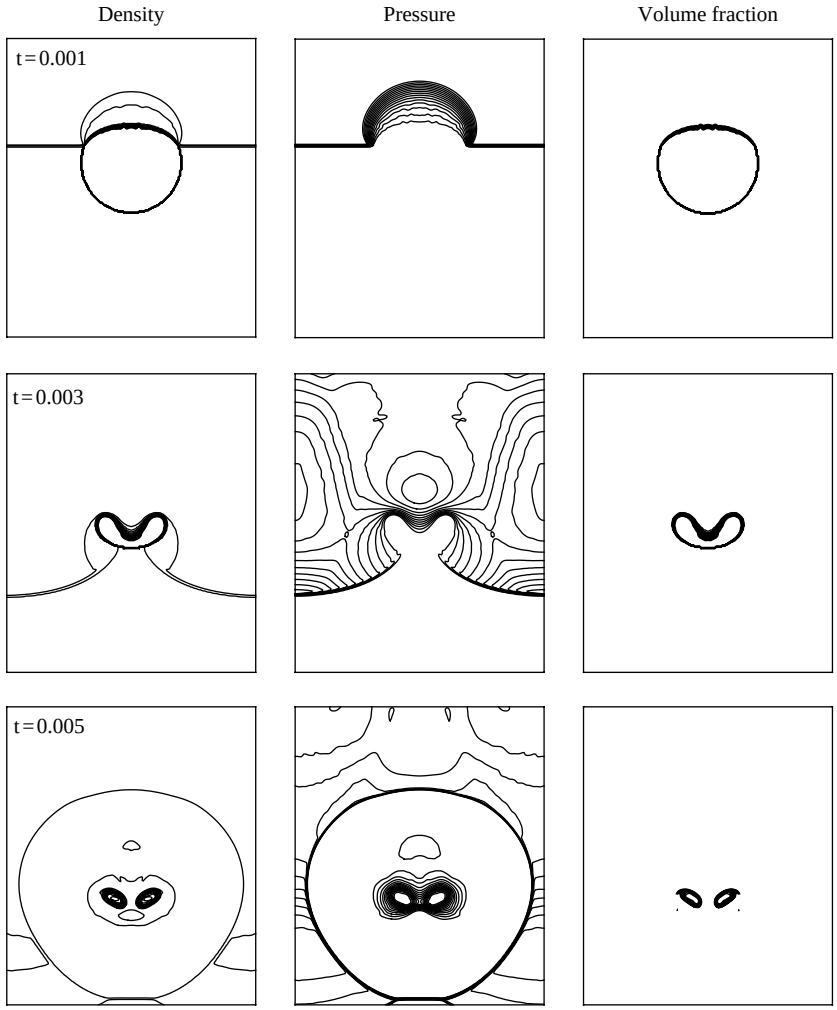

Note: Here a 200×240 mesh grid is used

Figure 9.
Contours of the density, pressure and volume fraction for the problem of shock wave interactions with an air bubble

penetrating the bubble and complex systems of waves such as transmitted shock wave and reflected rarefaction wave are generated. At time $t = 0.003$, the shock continues moving downward, and the bubble has deformed greatly due to instability. At time $t = 0.005$, the bubble is divided into two vertexes. Our method gives good results, which compare well to those in Shyue (1999b).

6. Conclusion

In this paper, we present a third-order PPM scheme for the compressible two-fluid flows where the barotropic and nonbarotropic fluid components are separated by the material interfaces. We use the Tait and stiffened gas EOSs to characterize the

thermodynamic properties of the barotropic and nonbarotropic components, respectively. A mixture model system based on the volume fraction is introduced to model motions of the mixture. Based on the assumption of the equilibrium pressure and Shyue's idea, a mixture EOS is derived. We efficiently solve the model system by using the third-order Lagrangian-remapping version of PPM. As compared with other methods, the present scheme has two remarkable features. First, it can capture the material interfaces with less diffusions and without introducing spurious oscillations.

Second, this scheme can be easily extended to the multi-fluid flows and multidimensional implementations. Therefore, our method can be applied to a range of practical problems.

References

Abgrall, R. (1996), "How to prevent pressure oscillations in multicomponent flow calculations: a quasi conservative approach", *J. Comput. Phys*, Vol. 125, pp. 150-60.

Allaire, G., Clerc, S. and Kokh, S. (2002), "A five-equation model for the simulation of interfaces between compressible fluids", *J. Comput. Phys*, Vol. 181, pp. 577-616.

Brouillette, M. (2002), "The Richtmyer-Meshkov instability", *Annu. Rev. Fluid Mech.*, Vol. 34, pp. 445-68.

Colella, P. and Glaz, H.M. (1985), "Efficient solution algorithm for the Riemann problem for real gases", *J. Comput. Phys.*, Vol. 59, pp. 264-89.

Colella, P. and Woodward, P.R. (1984a), "The piecewise parabolic method for gas-dynamics simulation", *J. Comput. Phys.*, Vol. 54, pp. 174-201.

Colella, P. and Woodward, P.R. (1984b), "The numerical simulation of two-dimensional fluid flow with strong shocks", *J. Comput. Phys.*, Vol. 54, pp. 115-73.

Fedkiw, R.P., Aslam, T., Merriman, B. and Osher, S. (1999), "A non-oscillatory Eulerian approach to interfaces in multimaterial flows (the ghost fluid method)", *J. Comput. Phys.*, Vol. 152, pp. 457-92.

Johnsen, E. and Colonius, T. (2006), "Implementation of WENO schemes in compressible multicomponent flow problems", *J. Comput. Phys.*, Vol. 219, pp. 715-32.

Liu, T.G., Khoo, B.C. and Wang, C.W. (2005), "The ghost fluid method for compressible gas-water simulation", *J. Comput. Phys.*, Vol. 204, pp. 193-221.

Liu, T.G., Khoo, B.C. and Yeo, K.S. (2003), "Ghost fluid method for strong shock impacting on material interface", *J. Comput. Phys*, Vol. 190, pp. 651-81.

Ma, D.J., Sun, D.J. and Yin, X.Y. (2001), "Piecewise parabolic method for compressible flows of multifluids with high density ratio", *Chinese J. Comput. Phys.*, Vol. 12, pp. 517-22.

Nourgaliev, R.R., Dinh, T.N. and Theofanous, T.G. (2006), "Adaptive characteristics-based matching for compressible multifluid dynamics", *J. Comput. Phys.*, Vol. 213, pp. 500-29.

Perigaud, G. and Saurel, R. (2005), "A compressible flow model with capillary effects", *J. Comput. Phys.*, Vol. 209, pp. 139-78.

Shyue, K.M. (1998), "An efficient shock-capturing algorithm for compressible multicomponent problems", *J. Comput. Phys.*, Vol. 142, pp. 208-42.

Shyue, K.M. (1999a), "A fluid-mixture type algorithm for compressible multicomponent flow with van Der Waals equation of state", *J. Comput. Phys.*, Vol. 156, pp. 43-88.

Shyue, K.M. (1999b), "A volume-of-fluid type algorithm for compressible two-phase flows", *International Series of Numerical Mathematics*, Vol. 130, pp. 895-904.

Shyue, K.M. (2001), "A fluid-mixture type algorithm for compressible multicomponent flow with Mie-Grüneisen equation of state", *J. Comput. Phys.*, Vol. 171, pp. 678-707.

Shyue, K.M. (2004), "A fluid-mixture type algorithm for barotropic two-fluid flow problems", *J. Comput. Phys.*, Vol. 200, pp. 718-48.

Shyue, K.M. (2006), "A volume-fraction based algorithm for hybrid barotropic and non-barotropic two-fluid flow problems", *Shock Waves*, Vol. 15, pp. 407-23.

Strang, G. (1968), "On the construction and comparison of difference schemes", *SIAM J. Numer. Anal.*, Vol. 5 No. 3, pp. 506-17.

Thompson, P.A. (1972), *Compressible-fluid Dynamics*, McGraw-Hill, New York, NY.

Toro, E.F. (1999), *Riemann Solvers and Numerical Methods for Fluid Dynamics: A Practical Introduction*, Springer, Berlin Heidelberg.

van Brummelen, E.H. and Koren, B. (2003), "A pressure-invariant conservative Godunov-type method for barotropic two-fluid flows", *J. Comput. Phys.*, Vol. 185, pp. 289-308.

Corresponding author
J.G. Zheng can be contacted at: zhengjg9705@yahoo.com